Ultrafast Spectroscopic Signature of Charge Transfer between Single-Walled Carbon Nanotubes and C_{60}

Anne-Marie Dowgiallo,[†] Kevin S. Mistry,[†,‡] Justin C. Johnson,[†] and Jeffrey L. Blackburn[†,*]

[†]National Renewable Energy Laboratory, Golden, Colorado 80401, United States, and [‡]Physics Department, University of Colorado, Boulder, Colorado 80309, United States

ABSTRACT The time scales for interfacial charge separation and recombination play crucial roles in determining efficiencies of excitonic photovoltaics. Near-infrared photons are harvested efficiently by semiconducting single-walled carbon nanotubes (SWCNTs) paired with appropriate electron acceptors, such as fullerenes (*e.g.*, C_{60}). However, little is known about crucial photochemical events that occur on femtosecond to nanosecond time scales at such heterojunctions. Here, we present transient absorbance measurements that utilize a distinct spectroscopic signature of charges within SWCNTs, the absorbance of a trion quasiparticle, to measure both the ultrafast photoinduced electron transfer time (τ_{pet}) and yield (ϕ_{pet}) in photoexcited SWCNT−C_{60} bilayer films. The rise time of the trion-induced absorbance enables the determination of the photoinduced electron transfer (PET) time of $\tau_{pet} \leq 120$ fs, while an experimentally determined trion absorbance cross section reveals the yield of charge transfer ($\phi_{pet} \approx 38 \pm 3\%$). The extremely fast electron transfer times observed here are on par with some of the best donor:acceptor pairs in excitonic photovoltaics and underscore the potential for efficient energy harvesting in SWCNT-based devices.

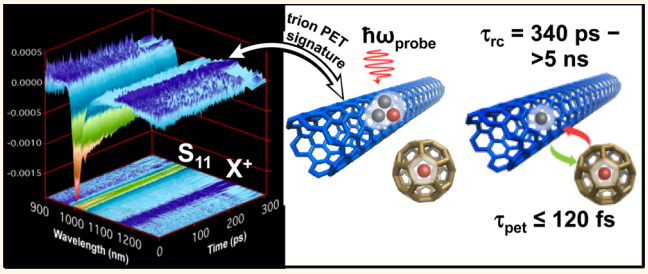

KEYWORDS: single-walled carbon nanotubes · fullerene · electron transfer · photovoltaic · charge generation · exciton dissociation · recombination · trion

Semiconducting single-walled carbon nanotubes (SWCNTs) are robust light absorbers that have garnered increasing attention as the electron-donating component in excitonic photovoltaic devices.[1,2] One such device consists of a thin film of chirality-sorted semiconducting SWCNTs paired with an electron-accepting layer of C_{60},[3−8] where internal quantum efficiencies exceeding 85%[3,8] and AM1.5 power conversion efficiencies of ∼1% (bilayer)[4] to 1.7% (bulk heterojunction)[5] have been achieved. In these devices, photoexcited SWCNT excitons are dissociated *via* interfacial photoinduced electron transfer (PET) to C_{60}. Time-resolved microwave conductivity (TRMC) measurements have revealed that the overlying C_{60} layer leads to an enhancement of long-lived mobile carriers (compared to a neat SWCNT film) when the s-SWCNTs are excited at their first excitonic transition (S_{11}).[9] However, TRMC has two important limitations—a temporal resolution of ∼4 ns and a sensitivity to *any* mobile charges—that make it difficult to unambiguously identify and temporally track charges associated with one phase (SWCNT or C_{60}), especially at times relevant to the initial PET step (presumably femtosecond or picosecond time-scale).

Distinct spectroscopic signatures of charges in semiconductors are important and ubiquitous tools for understanding ultrafast charge separation in excitonic photovoltaic active layers. Such signatures include free carrier induced absorption (IA) in oxides (*e.g.*, TiO_2),[10] polaronic IA in semiconducting polymers,[11,12] and intraband electron or hole IA in semiconductor quantum dots.[13,14] We hypothesized that it would be possible to quantitatively track ultrafast interfacial charge separation in SWCNT heterojunctions by using the spectroscopic signature of a three-body quasiparticle known as a trion.[15] In this case, we reasoned that the hole remaining on a SWCNT following PET (induced by a pump pulse) can bind to an exciton (generated by a probe pulse) to form a three-particle complex containing two holes and one electron. The resulting

* Address correspondence to Jeffrey.Blackburn@nrel.gov.

Received for review June 16, 2014 and accepted July 14, 2014.

Published online July 14, 2014
10.1021/nn503271k

© 2014 American Chemical Society

"positive trion", X^+, has a distinct optical absorption, providing an unambiguous signature of ultrafast PET.

Trions were first predicted in 1958 as stable quasiparticles in semiconductors,[16] were first observed experimentally in 1993 in semiconducting quantum wells,[17,18] and, more recently, have been predicted and observed in quantum dots[19,20] and semiconducting SWCNTs.[15,21−25] In SWCNTs, trion states of singlet excitons are predicted to have high binding energies, up to ∼14% of the exciton energy.[21] Stable trions have been demonstrated in SWCNTs by means of chemical doping,[15] electrochemical doping,[23] and optical excitation.[24,25] Due to the high trion binding energy, the trion absorption transition is significantly red-shifted with respect to the S_{11} (*e.g.*, $\Delta E \approx 170$ meV for (6,5)) and has typically been used as an indicator of ground-state charges. In ultrafast pump−probe experiments on SWCNTs at high photon fluences, excited-state charges can be generated through exciton Auger ionization processes, which can then form trions following subsequent photon absorption.[24] These optically generated trions appear as an IA that decays within hundreds of picoseconds.[24] In principle, the appearance and decay of the trion IA in transient absorbance (TA) measurements should reveal the temporal dynamics of charge separation and recombination in SWCNT−C_{60} systems.

In this study, we examine thin films of (6,5) SWCNTs both with and without an overlying C_{60} layer, using 1000 nm pump (resonant with S_{11}) and near-infrared probe TA spectroscopy. At low pump fluences ($\leq 3 \times 10^{12}$ photons pulse^{-1} cm^{-2}), we observe the trion IA around 1174 nm in the SWCNT−C_{60} bilayer, whereas no trion IA appears for the neat SWCNT film. The interfacial PET time constant (rise time of the trion IA) was determined to be ≤120 fs, which is limited by the instrument response of our TA system. In addition, very long lifetimes for the exciton bleach and trion IA in the SWCNT−C_{60} bilayer suggest efficient separation of opposite charges into the two phases, which inhibits carrier recombination. Trion generation is confirmed through steady-state absorption measurements of neat SWCNT films (without C_{60}) systematically doped by a p-type dopant. Quantitative calculations of the hole density in these doped SWCNTs allow for the determination of the absorption cross section of the trion, which in turn allows us to estimate the hole density and charge transfer yield ($\phi_{pet} \approx 38 \pm 3\%$) for SWCNT−$C_{60}$ films in the TA measurement. These results represent the first time the trion has been used as a distinct spectroscopic probe to quantify ultrafast photoinduced charge separation at a nanoscale heterojunction.

RESULTS AND DISCUSSION

For this study, we prepared nearly monochiral (6,5) SWCNT dispersions, using a fluorene-based polymer dispersant (PFO-BPy). Thin films of (6,5) SWCNTs (∼9 nm) were prepared with and without an overlying C_{60} layer of approximately 50 nm on quartz substrates. The neat SWCNT film has a strong absorbance peak at 1000 nm corresponding to the S_{11} transition of the (6,5) SWCNT (Figure 1a).

Other notable absorption features include the K-momentum phonon sideband (X_1) at 862 nm[26] and second excitonic transition (S_{22}) at 574 nm. The (6,5) SWCNT solution used to prepare the thin films also contained small amounts of (7,6), (7,5), and (6,4) minority species, which were identified using photoluminescence excitation (PLE) spectroscopy (Figure 1b). In the SWCNT−C_{60} film, the S_{11} peak is red-shifted due to an increase in the local dielectric constant from the C_{60} layer. An absorbance shoulder of C_{60} can be observed at ∼420 nm, and some scattering by the C_{60} layer induces a positive offset of the bilayer spectrum.

In the bilayer, PET occurs at the interface between the SWCNT and C_{60} films due to a sufficient thermodynamic driving force of the type II heterojunction present between the (6,5) SWCNT and C_{60}.[9,27] To elucidate the PET time constant, TA spectra were collected for the SWCNT and SWCNT−C_{60} thin films, pumping at the S_{11} transition of (6,5) nanotubes (1000 nm) and probing in the near-infrared (900−1300 nm). For the SWCNT film, a strong bleach of the S_{11} exciton transition appears at 1004 nm and recovers completely within ∼1 ns (90% recovery within ∼20 ps, Figure 1c). Bleaching of the S_{11} transition in photoexcited (6,5) SWCNTs occurs because of both phase-space filling and Coulomb interaction between excitons.[24] In contrast, the S_{11} bleach occurs at 1008 nm for the SWCNT−C_{60} film (Figure 1d) and persists for the full length of our experimental resolution (5.6 ns). The red-shift of the bilayer S_{11} bleach results from an increased local dielectric constant from the presence of C_{60} and is consistent with Figure 1a. In addition, an IA arises at ∼1174 nm at times immediately following the pump pulse and persists for the entire 5.6 ns experimental window (Figure 1d). We attribute this new long-lived peak to the absorbance of positive trions (X^+) following PET at the SWCNT−C_{60} interface; in this case, holes remaining on the SWCNT after PET bind to excitons generated by the probe pulse. This IA is shifted by 174 meV from S_{11}, consistent with previous observations of trions generated (*via* exciton Auger ionization) in (6,5) SWNCTs in TA experiments[24] or luminescence of (6,5) SWCNTs doped with ground-state holes or electrons.[15,23] Figure 1e demonstrates the stark contrast between the TA spectra of the SWCNT and SWCNT−C_{60} films at long pump−probe delays (*e.g.*, 300 ps). At these long delays, the neat film displays only a very weak bleach signal, whereas the bilayer film displays a strong S_{11} bleach and X^+ IA.

It is important to note that the trion IA is not observed for the neat SWCNT film (Figure 1c), even at early times. This result is consistent with previous TA measurements where the trion IA was not observed

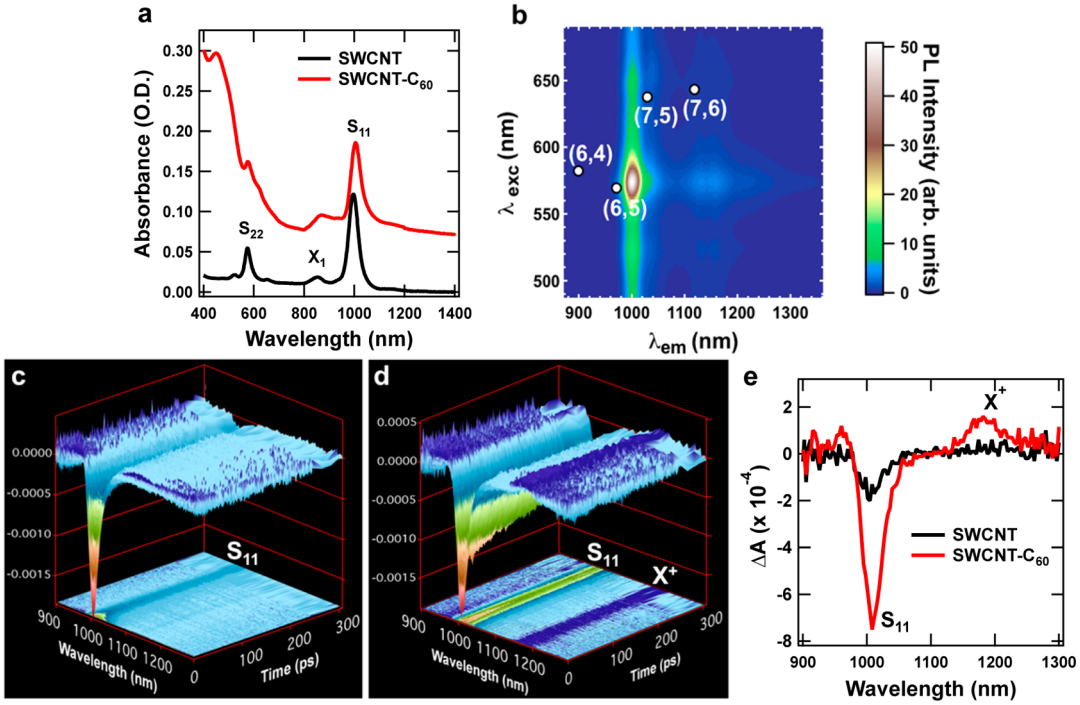

Figure 1. (a) Linear absorption spectra of the thin films of (6,5) SWCNT before (black) and after (red) C_{60} deposition. (b) Photoluminescence excitation (PLE) map of (6,5) SWCNT solution after removal of ~99% of the PFO-BPy polymer, with the minority nanotube species labeled. Differential absorption spectra for a thin film of (c) (6,5) SWCNT and (d) (6,5) SWCNT−C_{60} for the first 300 ps after time zero following excitation at the S_{11} excitonic transition. The trion (X^+) peak appears in the SWCNT−C_{60} film at 1174 nm (purple stripe) in (d). (e) Comparison of the differential absorption spectra of the SWCNT (black trace) and SWCNT−C_{60} (red trace) films at a delay time of 300 ps. The pump fluence for (c) through (e) is 3×10^{12} photons pulse^{-1} cm^{-2} (0.006 exciton nm^{-1}).

for (6,5) SWCNTs in solution for pump fluences below 5×10^{12} photons pulse^{-1} cm^{-2}.[24] In those experiments, a trion IA was observed only at sufficiently high pump fluences (5×10^{12} to 2.5×10^{14} photons pulse^{-1} cm^{-2}) due to the fact that large exciton densities result in collision-induced exciton Auger ionization, where an exciton is dissociated into free carriers that can then bind to excitons (from the probe pulse) to form trions.[24] In our experiments, we used low pump fluences (<3×10^{12} photons pulse^{-1} cm^{-2}) to remain within the regime where the differential absorption intensity of S_{11} increases linearly with pump fluence (Figure S1) and where the trion IA is absent for the neat SWCNT film. At early times (~100 fs), there is a broad, short-lived peak centered at 1130 nm ($\Delta E \approx$ 130 meV) for the neat SWCNT film that decays within ~5 ps (Figure S2a), which has previously been assigned to biexciton formation.[24,28] Figure S2 demonstrates that the S_{11} bleach and 1130 nm biexciton IA arise from the same (6,5) exciton population in the neat film and that the biexciton feature contributes minimally to spectra observed for the photoexcited bilayer. We also note that charge transfer, and subsequent trion formation, is not expected to occur between the photoexcited SWCNT and ground-state polymer (PFO-BPy) because large-band-gap polyfluorene polymers are expected to form a type I heterojunction with semiconducting SWCNTs.[29,30] The high PL intensity of the PFO-BPy (6,5) SWCNT dispersion (Figure 1b) and lack of a trion IA in the neat SWCNT sample (Figure 1c) further confirm that charge transfer from SWCNTs to PFO-BPy does not occur.

The decay kinetics of the S_{11} bleach for both the SWCNT (black traces) and SWCNT−C_{60} (red traces) films are shown in Figure 2a. It can readily be seen that the S_{11} bleach recovers at a faster rate in the neat SWCNT film compared to that of SWCNT−C_{60}. The decays are fit to a sum of three exponentials convoluted with our instrument response function (~120 fs, Figure S3).

At early times, the bleach kinetics in the SWCNT film are dominated by a fast decay, followed by two longer lifetimes (150 fs, 2.5 ps, and 23 ps, black fit line). A similar fit to the bilayer film (red fit line) reveals that the two shortest time constants associated with *exciton decay* are reduced to ~112 fs and 1.9 ps, as a result of the competing electron transfer decay pathway. A third time constant of ~290 ps is necessary to fit the data; a fit of the trion IA (Figure 2d, *vide infra*) indicates that this time constant represents the decay of the *charge population* resulting from PET. Figure 2b demonstrates that the bleach for the SWCNT film is fully recovered by 1.2 ns, whereas the S_{11} bleach persists in the SWCNT−C_{60} film beyond 5.6 ns. This long-lived bleach results directly from the *charge population* (*i.e.*, Pauli blocking) that now resides on the SWCNTs following PET, with the long decay times reflecting the

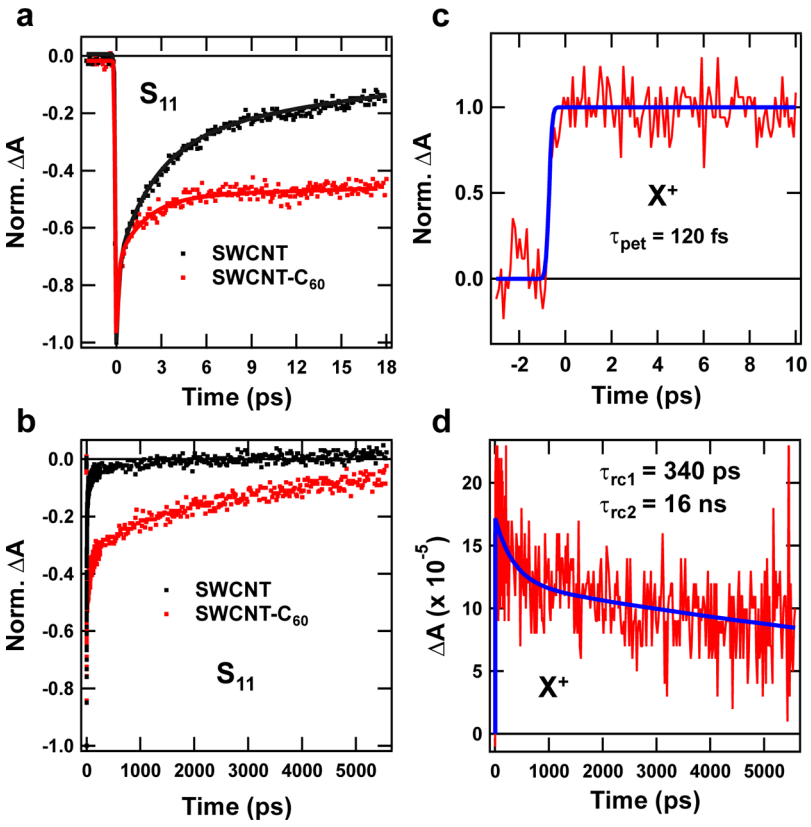

Figure 2. (a) Normalized transients of S_{11} exciton bleach for SWCNT (black, λ_{probe}: 1004) and SWCNT−C_{60} films (red, λ_{probe}: 1008 nm) at early times. The red and black lines correspond to three-exponential fits to the raw kinetic traces (see text). (b) Bleach decay dynamics for SWCNT (black) and SWCNT−C_{60} (red) for full experimental window (out to 5.6 ns). (c) Normalized X^+ trion IA at 1174 nm. Blue line is an integrated Gaussian fit, giving a rise time of ~120 fs. (d) Full kinetic trace for the X^+ trion IA, with its corresponding biexponential fit (blue line). The laser pump fluence for all panels is 3×10^{12} photons pulse^{-1} cm^{-2} (0.006 exciton nm^{-1}).

inhibition of carrier recombination due to charge separation in two distinct phases. Ultimately, the bleach dynamics are quite complex since a bleach arises from both charges and excitons, and furthermore a nonunity exciton dissociation yield (*vide infra* and refs 3, 4, 8, and 9) implies two populations of excitons are probed: (1) excitons that decay with the intrinsic kinetics of a neat SWCNT film and (2) excitons that decay due to photoinduced electron transfer. This complexity underscores the advantage of tracking PET with a signature that is sensitive *only to the presence of charges*.

Since the trion IA indicates the presence of charges created by pump-induced interfacial charge separation (with no contribution of excitons), the rise time of the trion IA (Figure 2c) is a clean measure of the PET time (τ_{pet}), with the decay (Figure 2d) representing charge recombination (τ_{rc}). The blue line in Figure 2c shows an integrated Gaussian fit of the trion rise time that reveals $\tau_{pet} \approx 120$ fs. This fast rise time indicates rapid electron injection into the C_{60} layer in the bilayer film ($\tau_{pet} \leq 120$ fs, IRF (instrument response function)-limited), where excitons are readily dissociated at the interface and the remaining holes on the SWCNTs form trions with excitons created by the probe pulse. The trion IA rise times and corresponding fits for several different pump fluences ranging from 1.7 to 8.3 $\times 10^{12}$ photons pulse^{-1} cm^{-2} are displayed in Figure S4; all fits consistently return τ_{pet} values on the order of our IRF, with an average value of 125 $\pm$ 14 fs. Convolution of the IRF with a biexponential decay yields charge recombination time constants (τ_{rc}) of 340 ps and 16 ns, at 30% and 70% of the decay, respectively (blue fit line, Figure 2d). Since the majority of carriers recombine with a time constant that is considerably longer than our experimental resolution (5.6 ns), future TA experiments on microsecond time scales and TRMC studies will be employed to measure the full recombination kinetics. For completeness, early and long time transients of the neat SWCNT film at 1174 nm (shoulder of the biexciton IA) are shown in Figure S5.

The schematic in Figure 3a summarizes the process of trion formation in the SWCNT−C_{60} bilayer that enables us to track charge generation: (1) formation of SWCNT excitons by the pump pulse; (2) dissociation of the excitons at the SWCNT−C_{60} interface by PET to the C_{60} layer; and (3) direct optical excitation (IA) of trions in the SWCNT by the probe pulse.

Importantly, analysis of the trion IA kinetics in Figure 2 reveals two very important photophysical phenomena for SWCNT−C_{60} heterojunctions: (1) exciton dissociation

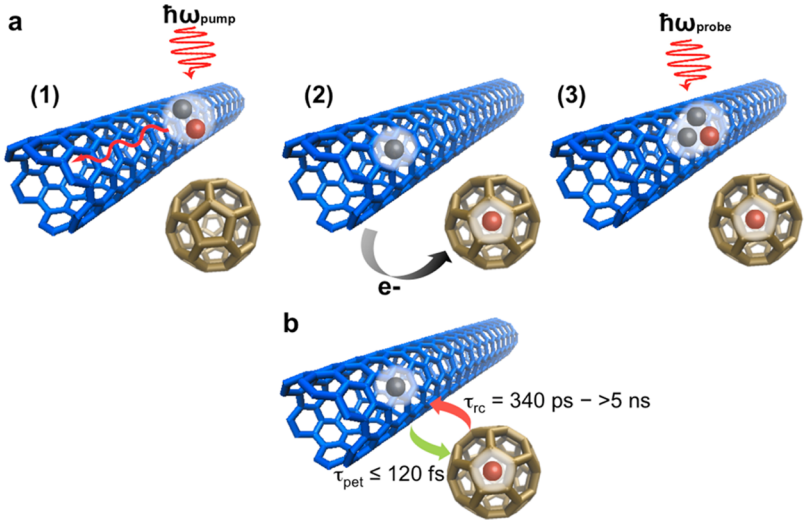

Figure 3. (a) Schematic of trion formation in the SWCNT−C_{60} film examined in this study involving (1) exciton generation in the SWCNT induced by the pump pulse, (2) exciton dissociation resulting from electron transfer from the SWCNT to C_{60}, and (3) optical excitation of a trion by the probe pulse. (b) Schematic summarizing the measured ultrafast electron transfer time from the SWCNT to C_{60}, followed by slow carrier recombination.

occurs with an extremely fast time constant of $\tau_{pet} \leq 120$ fs, and (2) electron−hole recombination across the SWCNT−C_{60} interface occurs on much slower time scales (hundreds of ps to >5 ns) (Figure 3b).

Our assignment of the trion IA in the TA measurement is confirmed through systematic doping of neat SWCNT films using the p-type dopant triethyloxonium hexachloroantimonate (OA),[31] producing a new peak in steady-state absorption at the trion energy (1.063 eV, 1166 nm). OA acts as a single-electron oxidant, where charge transfer from SWCNTs to bound $SbCl_6^-$ ions creates holes in the SWCNT valence band.[31] The amount of adsorbed OA was varied to controllably vary the hole density from 0.04 to 0.28 nm^{-1} (*vide infra*), with increasing hole density producing a concomitant decrease in the S_{11} and increase in the X^+ intensities (Figure 4a). Bleaching of the exciton transition occurs because of (1) state filling due to doped holes and (2) reduction in the exciton binding energy due to screening of the electron−hole Coulomb attraction. Absorption spectra of the hole-doped SWCNTs were fit with a series of Voigt peaks, corresponding to the (6,5) S_{11} and X^+ transitions, and other minority SWCNT S_{11} transitions. Figure 4b shows the absorption spectrum and corresponding Voigt peaks for the doped SWCNT film at a hole density of 0.08 nm^{-1}, while the Voigt analysis for the other doped samples is shown in Figure S6.

The inset in Figure 4b demonstrates a direct correlation between the S_{11} bleach (increased $\Delta T/T$) and the X^+ absorbance (increased $\Delta A/A$) as the hole density increases within the film, indicating a transfer of oscillator strength from the exciton transition to the trion transition. For comparison, the trion peak from steady-state absorption measurements is plotted with the trion IA from TA measurements in Figure 4c (green and black dots, respectively), along with Voigt fits (solid green and black lines, identical fwhm). An 11 meV red-shift of the trion IA in TA measurements of bilayers, relative to the steady-state measurements of doped neat films, is consistent with the 13 meV red-shift of the S_{11} bleach, since both shifts result from an increase of the local dielectric constant of SWCNTs due to the presence of C_{60}. Thus, Figure 4 confirms that the ~1174 nm IA observed in TA measurements on the bilayer sample is consistent with the trion optical transition induced by chemical hole doping and can be attributed to probe-induced trion formation.

Voigt analysis of films doped in the ground state with controlled hole densities allows us to calculate a calibration constant (trion cross section, σ_{X+}) for transforming X^+ peak intensities in TA measurements to hole densities in SWCNT−C_{60} bilayer films following PET. In turn, since the absorbed photon flux controls the initial exciton density in the SWCNT layer, we can calculate the important quantity of interfacial exciton dissociation yield. The hole density (N_h) induced by OA doping was estimated using an equation described by Matsuda *et al.*[32] that relates the change in S_{11} absorption intensity to the injected hole density (N_h):

$$1 - \frac{A_d}{A_0} = \left(1 - \sqrt{1 - \frac{\delta}{E_{bin}(0)}\sqrt{N_h}}\right) + \frac{N_h}{N_0} \quad (1)$$

In eq 1, A_0 and A_d are the integrated absorbance intensities before and after doping, N_0 is the hole density at which the S_{11} is completely bleached in SWCNTs, and $\delta/E_{bin}(0)$ describes the screening-induced reduction in exciton binding energy (taken here as ~0.88, previously calculated).[33] N_0 was estimated to be ~1.22 nm^{-1} for the (6,5) SWCNTs using the relationship

$$N_0 = \frac{4}{\pi\hbar}\sqrt{2m_h E_{bin}(0)} \quad (2)$$

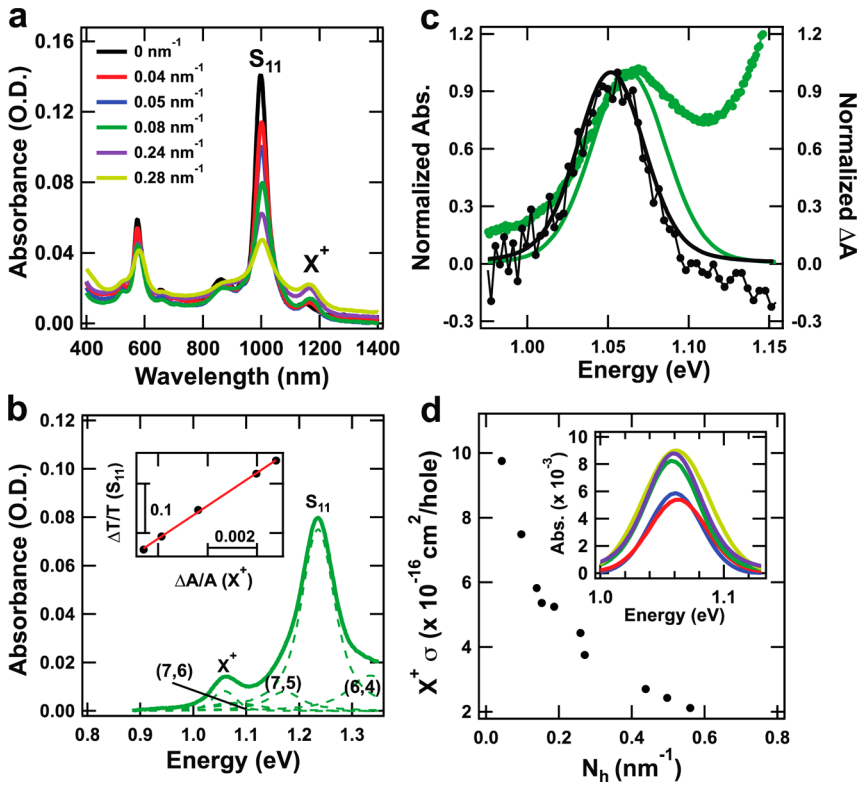

Figure 4. (a) Absorption spectra of progressively OA-doped SWCNT films with their corresponding hole densities (nm^{-1}). (b) Multipeak fit of the absorption spectrum of the doped sample with a hole density of 0.08 nm^{-1} using Voigt function analysis. The S_{11}, X^+, and other nanotube species are indicated. The S_{11} and X^+ intensities obtained after fitting each doped sample to the Voigt function were used to determine the relative change in the transmittance of the S_{11} ($\Delta T/T$) and the absorbance of X^+ ($\Delta A/A$) (inset). (c) Normalized absorbance of the trion after OA doping (green dots) and after pump laser excitation at 3 × 10^{12} photons pulse^{-1} cm^{-2} (black dots). The solid lines are Voigt fits to each peak. (d) Trion absorption cross section (σ) as a function of hole density for several doped nanotube films. The inset shows the Voigt peak fits of the trion peak for different doping levels.

where m_h is the hole effective mass ($\approx 0.14m_e$, where m_e is the mass of an electron) and $E_{bin}(0)$ is the exciton binding energy (278 meV for (6,5) SWCNTs, normalized to $\varepsilon \approx 4$).[34,35]

A calibration curve of $\Delta A/A$ (S_{11}) *versus* hole density (Figure S7a) was generated using eqs 1 and 2 to determine the experimental hole density, N_h, imparted by various OA doping levels. Next, the X^+ peaks obtained from the Voigt analysis (inset, Figure 4d) were used to correlate trion peak intensity (OD_{X+}) with the hole density imparted by various OA doping levels (Figure S7b). In Figure S7b, the optical density of the X^+ peak was normalized by the optical density of the S_{11} peak to allow for the analysis of SWCNT films with arbitrary thicknesses. Additionally, an S_{11} absorbance cross section of 2 × 10^{17} cm^2/C atom was used to calculate the trion absorbance cross section, σ_{X+}, as a function of N_h (Figure 4d). In the OA-doped films, the trion intensity grows sublinearly with increasing hole density (Figure S7b), begins to saturate at ~0.3 nm^{-1}, and by 0.5 nm^{-1} is completely saturated. At a hole density of 0.5 nm^{-1}, or equivalently 1 hole per 2 nm length of tube, the saturation behavior is consistent with the measured exciton size of 2.0 ± 0.7 nm in (6,5) SWCNTs.[36] Hence, the exciton occupies a space where only one hole would be able to bind to form a trion, and any additional holes present would not form a trion.

An empirical exponential fit to the data in Figure S7b is given by

$$\frac{OD_{X^+}}{OD_{S_{11}}} = 0.0674 - 0.0676e^{-21.5N_h} \quad (3)$$

and was used to calculate the hole density, $N_h(X^+)$, generated in TA measurements on the SWCNT−C_{60} film. Using eq 3, the hole density, $N_h(X^+)$, generated in SWCNTs following S_{11} excitation (and subsequent interfacial PET) in TA measurements can be determined by the trion IA intensity (ΔA_{X+}), which is normalized by the S_{11} intensity of the neat SWCNT film ($\Delta A_{X+}/OD_{S11}$).

Using the initial exciton density ($N_{ex} = I_0F_A$, where I_0 is the incident photon density and F_A is the fraction of absorbed light) introduced into SWCNTs from the pump pulse, we can calculate the yield of interfacial charge transfer, ϕ_{pet} where $\phi_{pet} = N_h/I_0F_A$. The resulting charge transfer yields are given in Table 1, with an average being 38 ± 3%.

The method described here should enable the measurement of photoinduced charge transfer (electron or hole) to or from any SWCNT species, as long as spectral congestion (from other SWCNTs or from features of the complementary donor or acceptor) does not interfere

TABLE 1. Hole Densities and Charge Transfer Yields

power (nW)	N_{ex} (nm^{-1})	$N_h(X^+)$ (nm^{-1})	ϕ_{pet}
70	0.0026	0.0011	0.41
90	0.0033	0.0012	0.36
110	0.0041	0.0014	0.34
130	0.0048	0.0019	0.39

with the observation of the trion IA. As a demonstration, TA measurements were also performed on (7,5) SWCNT and SWCNT−C_{60} bilayer films. A trion IA also appeared in the differential absorption spectra of the (7,5) SWCNT−C_{60} film at 1230 nm (shifted by 170 meV with respect to the S_{11} bleach), consistent with reports of the energy shift between S_{11} and X^+ for electrochemically doped (7,5) SWCNTs.[23] The kinetics of the S_{11} bleach and X^+ IA (Figure S8) were qualitatively similar to that of the (6,5) films, indicating ultrafast PET and slow charge recombination.

CONCLUSIONS

We demonstrate the first temporal resolution of ultrafast (≤120 fs) exciton dissociation at a SWCNT:fullerene interface by utilizing probe−pulse-induced trion formation as a transient spectroscopic signature of the resulting charges. The strategies developed here may prove beneficial for quantifying charge separation in a broad range of semiconductor systems with sufficient trion binding energies, such as single-layer MoS_2,[37] and can also probe PET for a number of other technologically interesting applications (*e.g.*, solar fuel production and catalysis). The fast PET times between SWCNTs and C_{60} and are on par with some of the best donor:acceptor pairs currently used in excitonic photovoltaics and are consistent with low reorganization energies and/or strong electronic coupling. Technologically, our results suggest tremendous potential for SWCNT−C_{60} heterojunctions in applications such as thin-film photovoltaics.

METHODS

SWCNTs produced by the CoMoCat method (SG65i) were purchased from Southwest Nanotechnologies, and poly-[(9,9-dioctylfluorenyl-2,7-diyl)-*alt-co*-(6,60-[2,20-bipyridine])] (PFO-BPy) was purchased from American Dye Source. SWCNTs were dispersed in ∼2.5 mg/mL PFO-BPy in toluene through tip sonication (1/2 in. probe) for 30 min at 40% intensity (Cole-Palmer CPX 750) in a bath of cool (18 °C) flowing water. The dispersion was then centrifuged for 5 min using an SW32Ti rotor (Beckman) at 13 200 rpm and 20 °C. The supernatant, containing predominantly (6,5) SWCNTs, was removed for further processing, and the pellet was discarded. The (6,5) SWCNT dispersion was then centrifuged for 20 h at 24 100 rpm and 0 °C to remove excess polymer. In this case, the resulting supernatant (containing free solution-phase polymer) was discarded, and the pellet (containing the (6,5) SWCNT material) was redispersed in toluene. This polymer removal process was repeated twice until a 1:1 SWCNT:PFO-BPy mass ratio was obtained.

Next, the (6,5)-enriched SWCNT dispersion was used to prepare thin SWCNT films on quartz substrates (22 mm × 10 mm × 1 mm). The substrates were cleaned prior to film deposition by sonication in separate baths of toluene and acetone and were then exposed to oxygen plasma for 5 min. Films were prepared through ultrasonic spray deposition[38] using a dispersion flow rate of 0.25 mL/min and gas flow rate of 7.0 std L/min. The nozzle power was fixed at 0.8 W, and the substrate was heated to 130 °C to allow for evaporation of the solvent. After spraying the films, they were soaked in a hot toluene bath (80 °C) to remove some residual polymer and better couple SWCNTs within the film. A thin layer of C_{60} (∼50 nm) was deposited on SWCNT films *via* thermal evaporation at a pressure of $<1 \times 10^{-6}$ Torr and a deposition rate of 0.5 Å/s. In order to ensure the SWCNT and SWCNT−C_{60} films were in an inert atmosphere during the transient absorption experiments, the quartz slide containing the samples was introduced into a helium glovebox, and another quartz slide was sealed on top of the sample using a polymer film (Surlyn, Solaronix) heated to 90 °C. The polymer was cut into a hollow frame so that it sealed only the outer edges of the slide and did not interfere with the sample.

In order to dope neat (6,5) SWCNT films (for Figure 4), solutions of triethyloxonium hexachloroantimonate in dichloroethane were prepared using a method described by Chandra *et al.*[31] with the following concentrations: 0.001, 0.01, and 0.1 mg/mL. The films were soaked in these solutions for 1 h at 70 °C and then dipped in acetone to remove excess dopant. Soaking in the 0.001, 0.01, and 0.1 mg/mL OA solutions resulted in hole densities of 0.05, 0.24, and 0.28 nm^{-1}, respectively. The doped films with hole densities of 0.05 and 0.24 nm^{-1} were allowed to sit for approximately 1 h to produce hole densities of 0.04 and 0.08 nm^{-1}, respectively.

Steady-state absorbance measurements were carried out on a Varian Cary 500 spectrophotometer. The thickness of each layer was estimated using the optical density of the S_{11} at 1000 nm and the C_{60} peak at 422 nm (absorption coefficient, 1.21×10^5 cm^{-1}).[4,39] PLE maps were acquired using a home-built Fourier transform spectrometer.[40] Femtosecond pump−probe TA experiments were performed on a 1 kHz regeneratively amplified Ti:sapphire laser system that produces 4 mJ laser pulses at 800 nm. The Ti:sapphire laser pumps an optical parametric amplifier to generate 1000 nm light, which was chopped at a rate of 500 Hz and used as the excitation pump pulse. Passing a portion of the amplified 800 nm light through a sapphire plate generated a near-infrared continuum probe pulse (800 nm < λ_{probe} < 1700 nm). The probe pulses were delayed in time with respect to the pump pulse using a motorized translation stage mounted with a retroreflecting mirror. The pump and probe beams were spatially overlapped at the quartz slide, and the sample was excited through the nanotube layer first. Typical averaging times for data collection were 5−8 s, at each pump−probe delay, to achieve high signal-to-noise ratios. The instrument response function was determined by measuring the nonresonant response of the pump and probe pulses in ZnSe (Figure S3). At 1115 nm, a Gaussian fit yielded an instrument response time of 117 ± 5 fs. The probe beam was spectrally dispersed on an InGaAs detector that has a sensitivity range of 800−1600 nm. The measurements were carried out from 3 ps before time zero to 5.6 ns after time zero. The excitation pulse energies used ranged from 0.14 to 1 nJ $pulse^{-1}$.

Conflict of Interest: The authors declare no competing financial interest.

Supporting Information Available: Fluence dependence of S_{11} bleach for neat (6,5) SWCNT film, differential absorption spectra showing biexciton IA in neat film, instrument response function for transient absorption technique, rise time fits of the trion peak at different pump fluences, transients for the neat (6,5) SWCNT film at 1174 nm, Voigt analysis of OA-doped SWCNT films, hole density calibration curves, and transient absorption data on neat (7,5) SWCNT and (7,5) SWCNT−C_{60}

films. This material is available free of charge *via* the Internet at http://pubs.acs.org.

Acknowledgment. This work was supported by the Solar Photochemistry Program of the U.S. Department of Energy, Office of Science, Basic Energy Sciences, Division of Chemical Sciences, Geosciences and Biosciences, under Contract No. DE-AC36-08GO28308 to NREL.

REFERENCES AND NOTES

1. Arnold, M. S.; Blackburn, J. L.; Crochet, J. J.; Doorn, S. K.; Duque, J. G.; Mohite, A.; Telg, H. Recent Developments in the Photophysics of Single-Walled Carbon Nanotubes for Their Use as Active and Passive Material Elements in Thin Film Photovoltaics. *Phys. Chem. Chem. Phys.* **2013**, *15*, 14896–14918.
2. D'Souza, F.; Ito, O. Photosensitized Electron Transfer Processes of Nanocarbons Applicable to Solar Cells. *Chem. Soc. Rev.* **2012**, *41*, 86–96.
3. Bindl, D. J.; Wu, M.-Y.; Prehn, F. C.; Arnold, M. S. Efficiently Harvesting Excitons from Electronic Type-Controlled Semiconducting Carbon Nanotube Films. *Nano Lett.* **2010**, *11*, 455–460.
4. Shea, M. J.; Arnold, M. S. 1% Solar Cells Derived from Ultrathin Carbon Nanotube Photoabsorbing Films. *Appl. Phys. Lett.* **2013**, *102*, 243101.
5. Ye, Y.; Bindl, D. J.; Jacobberger, R. M.; Wu, M.-Y.; Roy, S. S.; Arnold, M. S. Semiconducting Carbon Nanotube Aerogel Bulk Heterojunction Solar Cells. *Small* **2014**, Early View, DOI: 10.1002/smll.201400696.
6. Jain, R. M.; Howden, R.; Tvrdy, K.; Shimizu, S.; Hilmer, A. J.; McNicholas, T. P.; Gleason, K. K.; Strano, M. S. Polymer-Free near-Infrared Photovoltaics with Single Chirality (6,5) Semiconducting Carbon Nanotube Active Layers. *Adv. Mater.* **2012**, *24*, 4436–4439.
7. Ramuz, M. P.; Vosgueritchian, M.; Wei, P.; Wang, C.; Gao, Y.; Wu, Y.; Chen, Y.; Bao, Z. Evaluation of Solution-Processable Carbon-Based Electrodes for All-Carbon Solar Cells. *ACS Nano* **2012**, *6*, 10384–10395.
8. Bindl, D. J.; Arnold, M. S. Efficient Exciton Relaxation and Charge Generation in Nearly Monochiral (7,5) Carbon Nanotube/C60 Thin-Film Photovoltaics. *J. Phys. Chem. C* **2013**, *117*, 2390–2395.
9. Bindl, D. J.; Ferguson, A. J.; Wu, M.-Y.; Kopidakis, N.; Blackburn, J. L.; Arnold, M. S. Free Carrier Generation and Recombination in Polymer-Wrapped Semiconducting Carbon Nanotube Films and Heterojunctions. *J. Phys. Chem. Lett.* **2013**, *4*, 3550–3559.
10. Ellingson, R. J.; Asbury, J. B.; Ferrere, S.; Ghosh, H. N.; Sprague, J. R.; Lian, T.; Nozik, A. J. Dynamics of Electron Injection in Nanocrystalline Titanium Dioxide Films Sensitized with $[Ru(4,4'\text{-dicarboxy-}2,2'\text{-bipyridine})_2(NCs)_2]$ by Infrared Transient Absorption. *J. Phys. Chem. B* **1998**, *102*, 6455–6458.
11. Kraabel, B.; Lee, C. H.; McBranch, D.; Moses, D.; Sariciftci, N. S.; Heeger, A. J. Ultrafast Photoinduced Electron Transfer in Conducting Polymer-Buckminsterfullerene Composites. *Chem. Phys. Lett.* **1993**, *213*, 389–394.
12. Brabec, C. J.; Zerza, G.; Cerullo, G.; De Silvestri, S.; Luzzati, S.; Hummelen, J. C.; Sariciftci, S. Tracing Photoinduced Electron Transfer Process in Conjugated Polymer/Fullerene Bulk Heterojunctions in Real Time. *Chem. Phys. Lett.* **2001**, *340*, 232–236.
13. Blackburn, J. L.; Selmarten, D. C.; Nozik, A. J. Electron Transfer Dynamics in Quantum Dot/Titanium Dioxide Composites Formed by in Situ Chemical Bath Deposition. *J. Phys. Chem. B* **2003**, *107*, 14154–14157.
14. Yang, Y.; Rodriguez-Cordoba, W.; Lian, T. Ultrafast Charge Separation and Recombination Dynamics in Lead Sulfide Quantum Dot-Methylene Blue Complexes Probed by Electron and Hole Intraband Transitions. *J. Am. Chem. Soc.* **2011**, *133*, 9246–9249.
15. Matsunaga, R.; Matsuda, K.; Kanemitsu, Y. Observation of Charged Excitons in Hole-Doped Carbon Nanotubes Using Photoluminescence and Absorption Spectroscopy. *Phys. Rev. Lett.* **2011**, *106*, 037404.
16. Lampert, M. A. Mobile and Immobile Effective-Mass-Particle Complexes in Nonmetallic Solids. *Phys. Rev. Lett.* **1958**, *1*, 450–453.
17. Kheng, K.; Cox, R. T.; d'Aubigné, M. Y.; Bassani, F.; Saminadayar, K.; Tatarenko, S. Observation of Negatively Charged Excitons X- in Semiconductor Quantum Wells. *Phys. Rev. Lett.* **1993**, *71*, 1752–1755.
18. Huard, V.; Cox, R. T.; Saminadayar, K.; Arnoult, A.; Tatarenko, S. Bound States in Optical Absorption of Semiconductor Quantum Wells Containing a Two-Dimensional Electron Gas. *Phys. Rev. Lett.* **2000**, *84*, 187–190.
19. Jha, P. P.; Guyot-Sionnest, P. Trion Decay in Colloidal Quantum Dots. *ACS Nano* **2009**, *3*, 1011–1015.
20. Patton, B.; Langbein, W.; Woggon, U. Trion, Biexciton, and Exciton Dynamics in Single Self-Assembled CdSe Quantum Dots. *Phys. Rev. B* **2003**, *68*, 125316.
21. Rønnow, T. F.; Pedersen, T. G.; Cornean, H. D. Stability of Singlet and Triplet Trions in Carbon Nanotubes. *Phys. Lett. A* **2009**, *373*, 1478–1481.
22. Rønnow, T. F.; Pedersen, T. G.; Cornean, H. D. Correlation and Dimensional Effects of Trions in Carbon Nanotubes. *Phys. Rev. B* **2010**, *81*, 205446.
23. Park, J. S.; Hirana, Y.; Mouri, S.; Miyauchi, Y.; Nakashima, N.; Matsuda, K. Observation of Negative and Positive Trions in the Electrochemically Carrier-Doped Single-Walled Carbon Nanotubes. *J. Am. Chem. Soc.* **2012**, *134*, 14461–14466.
24. Yuma, B.; Berciaud, S.; Besbas, J.; Shaver, J.; Santos, S.; Ghosh, S.; Weisman, R. B.; Cognet, L.; Gallart, M.; Ziegler, M.; *et al.* Biexciton, Single Carrier, and Trion Generation Dynamics in Single-Walled Carbon Nanotubes. *Phys. Rev. B* **2013**, *87*, 205412.
25. Santos, S. M.; Yuma, B.; Berciaud, S.; Shaver, J.; Gallart, M.; Gilliot, P.; Cognet, L.; Lounis, B. All-Optical Trion Generation in Single-Walled Carbon Nanotubes. *Phys. Rev. Lett.* **2011**, *107*, 187401.
26. Blackburn, J. L.; Holt, J. M.; Irurzun, V. M.; Resasco, D. E.; Rumbles, G. Confirmation of K-Momentum Dark Exciton Vibronic Sidebands Using ^{13}C-Labeled, Highly Enriched (6,5) Single-Walled Carbon Nanotubes. *Nano Lett.* **2012**, *12*, 1398–1403.
27. Arnold, M. S.; Zimmerman, J. D.; Renshaw, C. K.; Xu, X.; Lunt, R. R.; Austin, C. M.; Forrest, S. R. Broad Spectral Response Using Carbon Nanotube/Organic Semiconductor/C60 Photodetectors. *Nano Lett.* **2009**, *9*, 3354–3358.
28. Kammerlander, D.; Prezzi, D.; Goldoni, G.; Molinari, E.; Hohenester, U. Biexciton Stability in Carbon Nanotubes. *Phys. Rev. Lett.* **2007**, *99*, 126806.
29. Gomulya, W.; Gao, J.; Loi, M. A. Conjugated Polymer-Wrapped Carbon Nanotubes: Physical Properties and Device Applications. *Eur. Phys. J. B* **2013**, *86*, 1–13.
30. Stranks, S. D.; Yong, C.-K.; Alexander-Webber, J. A.; Weisspfennig, C.; Johnston, M. B.; Herz, L. M.; Nicholas, R. J. Nanoengineering Coaxial Carbon Nanotube-Dual-Polymer Heterostructures. *ACS Nano* **2012**, *6*, 6058–6066.
31. Chandra, B.; Afzali, A.; Khare, N.; El-Ashry, M. M.; Tulevski, G. S. Stable Charge-Transfer Doping of Transparent Single-Walled Carbon Nanotube Films. *Chem. Mater.* **2010**, *22*, 5179–5183.
32. Mouri, S.; Matsuda, K. Exciton-Hole Interactions in Hole-Doped Single-Walled Carbon Nanotubes Evaluated by Absorption Spectral Changes. *Journal of Applied Physics* **2012**, *111*, 094309.
33. Spataru, C. D.; Léonard, F. Tunable Band Gaps and Excitons in Doped Semiconducting Carbon Nanotubes Made Possible by Acoustic Plasmons. *Phys. Rev. Lett.* **2010**, *104*, 177402.
34. Capaz, R. B.; Spataru, C. D.; Ismail-Beigi, S.; Louie, S. G. Excitons in Carbon Nanotubes: Diameter and Chirality Trends. *Phys. Status Solidi B* **2007**, *244*, 4016–4020.
35. Dukovic, G.; Wang, F.; Song, D.; Sfeir, M. Y.; Heinz, T. F.; Brus, L. E. Structural Dependence of Excitonic Optical Transitions and Band-Gap Energies in Carbon Nanotubes. *Nano Lett.* **2005**, *5*, 2314–2318.

36. Luer, L.; Hoseinkhani, S.; Polli, D.; Crochet, J.; Hertel, T.; Lanzani, G. Size and Mobility of Excitons in (6, 5) Carbon Nanotubes. *Nat. Phys.* **2009**, *5*, 54–58.
37. Mak, K. F.; He, K.; Lee, C.; Lee, G. H.; Hone, J.; Heinz, T. F.; Shan, J. Tightly Bound Trions in Monolayer MoS_2. *Nat. Mater.* **2013**, *12*, 207–211.
38. Tenent, R. C.; Barnes, T. M.; Bergeson, J. D.; Ferguson, A. J.; To, B.; Gedvilas, L. M.; Heben, M. J.; Blackburn, J. L. Ultrasmooth, Large-Area, High-Uniformity, Conductive Transparent Single-Walled-Carbon-Nanotube Films for Photovoltaics Produced by Ultrasonic Spraying. *Adv. Mater.* **2009**, *21*, 3210–3216.
39. Hebard, A. F.; Haddon, R. C.; Fleming, R. M.; Kortan, A. R. Deposition and Characterization of Fullerene Films. *Appl. Phys. Lett.* **1991**, *59*, 2109–2111.
40. McDonald, T. J.; Jones, M.; Engtrakul, C.; Ellingson, R. J.; Rumbles, G.; Heben, M. J. Near-Infrared Fourier Transform Photoluminescence Spectrometer with Tunable Excitation for the Study of Single-Walled Carbon Nanotubes. *Rev. Sci. Instrum.* **2006**, *77*, 053104.